

PAPER • OPEN ACCESS

Ways to increase the efficiency of detection of unmanned aerial vehicles by thermal imaging devices

To cite this article: Yu M Shmelov *et al* 2021 *IOP Conf. Ser.: Mater. Sci. Eng.* **1164** 012071

View the [article online](#) for updates and enhancements.

You may also like

- [Application-specific nuclear medical *in vivo* imaging devices](#)
Abhijit J Chaudhari and Ramsey D Badawi
- [Uncooled infrared thermal imaging sensor using vacuum-evaporated europium phosphor](#)
Min Wang, Takashiro Tsukamoto and Shuji Tanaka
- [Regions of interest selection and thermal imaging data analysis in sports and exercise science: a narrative review](#)
David Perpetuini, Damiano Formenti, Daniela Cardone et al.



The Electrochemical Society
Advancing solid state & electrochemical science & technology

242nd ECS Meeting

Oct 9 – 13, 2022 • Atlanta, GA, US

Abstract submission deadline: **April 8, 2022**

Connect. Engage. Champion. Empower. Accelerate.

MOVE SCIENCE FORWARD



Submit your abstract



Ways to increase the efficiency of detection of unmanned aerial vehicles by thermal imaging devices

Yu M Shmelov¹, O V Brusakova², R P Yakovlev¹ and M V Petchenko²

¹ Kremenchuk College of Aviation of Kharkiv National University of Internal Affairs, 39600, 17/6, vul. Peremogy Kremenchuk, Poltava region, Ukraine, 39600, 17/6, Peremogy str., Kremenchuk, Poltava reg., Ukraine

² Kharkiv National University of Internal Affairs, 61080, 27, Leo Landau ave. Kharkiv, Ukraine

Abstract. The possibilities to increase the efficiency of detection of air objects due to the optimized choice of a functional area of an infrared range of electromagnetic waves are mathematically estimated. It is shown that there is a need to use receivers with maximum visibility in longer wavelengths, as well as the need to work in the "transparency windows" of the atmosphere. With low visibility, long-wavelength infrared thermal imaging devices are advantageous at long distances from objects. Devices with more shortwave sensitivity can be effective over short distances. Radar detection methods in many cases are not able to detect small objects with a low reflection coefficient, which is one of the reasons for the small effective scattering area. Known methods of observation using night vision devices and thermal imaging devices, having their advantages, are also ineffective in certain conditions. An attempt is made to combine the advantages of detecting aerial objects by the multi-position radar method with the advantages of thermal imaging devices. A method of illuminating air objects with infrared searchlights is proposed, which implies the presence of many geometrically spaced sources of infrared radiation with a working spectrum combined with areas of "windows of transparency" of the atmosphere and the maximum sensitivity of the thermal imager. In such conditions, the receiver registers the total signal of thermal radiation of the object and the reflected rays of searchlights. Remote control of the spotlight emission, on which the effective scattering area depends linearly, makes it possible to bring it to the level guaranteed with a high probability of detecting a small flying object.

1. Introduction

In recent years, observations of hostilities in various hotspots of the planet show that unmanned aerial vehicles are experiencing a real boom. High combat efficiency of unmanned aerial vehicles confirms it as one of the most important types of aircraft. As a result, the problem of airspace control has become more acute. Modern technologies used in small aircraft, such as unmanned aerial vehicles (UAVs), dramatically reduce their visibility. Special methods and surveillance systems are needed for timely detection of UAVs. UAVs are of small size and special geometry, have low engine power, are made of composite structural materials, which is expressed in small effective area of electromagnetic wave scattering (EWS), perform covert flights at medium, low and extremely low altitudes and are often invisible to radar systems (RS). In addition, RSs are quite structurally complex, cumbersome and at high power dangerous to humans, energy-intensive, and also unmasked. The use of traditional pulse RSs to increase the probability of detection of UAVs requires radical changes in their physical and technical parameters, and hence in the structural elements, which results in an increase in the cost of their production and maintenance. Multi-position radiolocation with a specific arrangement of radars and receivers is more effective for detecting small targets [1-6]. However, spaced multi-position systems have a major drawback – loss of functionality in the absence of radio communication. To reliably detect a UAV, it is necessary to maintain a continuous radar field over the controlled area at low and extremely low altitudes.



The low visibility of UAVs and the limited possibilities to detect radars encourage the search for the possibility of detection by other unmasking features.

2. Literature analysis

Still new models with various possibilities and characteristics regularly appear on the UAV market, which requires immediate development of the theory and practice of combating them [7-8].

Trends in the development of small aircraft, ways to increase the probability of detection by the main types of visibility are analyzed [9-12]. Professional analysis of methods to increase the efficiency of UAV detection by traditional radio equipment showed that they are associated with an increase in the number of RSs, increasing power consumption [13-15]. Thus, to increase the effective scattering surface, the methods of single-position and multi-position radar are combined, for which the appropriate channels of synchronized processing of own signals and signals from third-party transmitters are formed in the RS. However, the developed recommendations for the optimal use of these systems do not reduce the financial costs of their production and operation [16-18].

One of the unmasking features of a UAV is thermal infrared (IR) radiation, which is mainly emitted by the power plant of the flying object. The possibility to be detected depends on the temperature contrast between the object and the background, the radiation area, the emissivity of materials. The targets in the IR region of the EMS are observed using night vision devices (NVD) and thermal imaging devices (TID). Each of them has its advantages and disadvantages. The use of active-pulse optoelectronic devices increases the detection range, but unmasks the observer. Such modern devices are complex in design and consume more energy [19-21].

Passive night vision devices are characterized by the covertness of reconnaissance surveillance and by their characteristics reach the theoretical limit of sensitivity [22-24]. Thermal imagers are inferior to night vision devices in resolution, but they can operate in complete darkness. Passive two-channel iconic optoelectronic systems are the most common for round-the-clock surveillance in poor visibility conditions [25-27].

Based on the problems of UAV detection, there is a need for a detailed study of the possibilities of increasing the detection efficiency in the IR range of EMS, the possibility of combining the methods of multi-position radar with the advantages of thermal imaging equipment.

2.1. Purpose of the paper.

Analyze possible mechanisms to increase the efficiency of detection of small aircraft TID.

3. Statement of the basic material

3.1. Optimization via the choice of the spectral section of the receiver sensitivity.

The efficiency of the system is its generalized functional property necessary to perform a certain task, which objectively expresses the degree of success in achieving the goal.

The signal-to-noise ratio at the output of the heat-sensitive radiation receiver is the physical and technical criterion of the efficiency of the TID observation.

The contrast of the thermal image of the object with temperature T_0 against the background with temperature T_ϕ is determined by difference signal ΔU [27-29]:

$$\Delta U_T = \frac{A_3 \cdot A_0}{\pi \cdot L^2} \cdot \int_0^\infty \tau_{oc}(\lambda) \cdot e^{-\alpha(\lambda)L} \cdot S_a(\lambda) \cdot [\varepsilon_0(\lambda)M(\lambda, T_0) - \varepsilon_\phi(\lambda) \cdot M(\lambda, T_\phi)] d\lambda, \quad (1)$$

where A_3 – the area of the entrance pupil of the optical system;

A_0 – the area of the object of observation;

λ – EMS length;

τ_{oc} – spectral transmittance of the optical system;

$\alpha(\lambda)$ – the natural indicator of the attenuation of the atmosphere;

$S_a(\lambda)$ – absolute voltage sensitivity of the radiation receiver;
 L – the distance between the object and the optical system;
 $\varepsilon_0(\lambda), \varepsilon_\phi(\lambda)$ – the coefficients of the radiation of the object and the background, respectively;
 $M(\lambda, T_0), M(\lambda, T_\phi)$ – the spectral density of the radiation of an absolutely black body at the object temperature T_0 and background temperature T_ϕ respectively;

$$M(\lambda, T) = c_1 \lambda^{-5} \left[\exp\left(\frac{c_2}{\lambda T}\right) - 1 \right]^{-1}, \text{ where } c_1 = 3.74 \cdot 10^{-16} \text{ W} \cdot \text{m}^2; c_2 = 1.439 \cdot 10^{-2} \text{ m} \cdot \text{K}.$$

Taking into account that $S_a(\lambda) = D_a^*(\lambda) \cdot \frac{U_u}{\sqrt{A_e \cdot \Delta f}} = D_{\max}^* \cdot D(\lambda) \cdot \frac{U_u}{\sqrt{A_e \cdot \Delta f}}$, expression (1) can be rewritten as follows:

$$\Delta U_T = \frac{A_3 \cdot A_0 \cdot U_u \cdot D_{\max}^*}{\pi \cdot L^2 \cdot \sqrt{A_e \cdot \Delta f}} \cdot \int_0^\infty \tau_{oc}(\lambda) \cdot e^{-\alpha(\lambda)L} \cdot D(\lambda) \cdot [\varepsilon_0(\lambda) \cdot M(\lambda, T_0) - \varepsilon_\phi(\lambda) \cdot M(\lambda, T_\phi)] d\lambda, \quad (2)$$

where $D_a^*(\lambda)$ – reduced detection ability, D_{\max}^* – its maximum value;

U_u – root-mean-square value of the noise;

Δf – equivalent noise bandwidth of the radiation receiver;

A_e – the area of the sensitive element of the receiver;

$D(\lambda) = \frac{D_a^*(\lambda)}{D_{\max}^*}$ – relative spectral detection ability.

To simplify the calculations, we make the following assumptions:

- integration $\tau_{oc}(\lambda)$ in expression (2) is substituted by an approximate value of the optical system transmittance integration coefficient τ_o ;
- assume $\varepsilon_0(\lambda) = \varepsilon_\phi(\lambda) = 1$;
- relative spectral detection ability $D(\lambda)$ is restricted by section $\lambda \in [\lambda_1, \lambda_2]$ within the limits of which $D(\lambda) = 1$;
- at low differences between the object temperature T_0 and background temperature T_ϕ the difference in expression (2) can be changed by temperature differential [37-38]:

$$d_T M(\lambda, T) = \frac{\partial M(\lambda, T)}{\partial T} dT \approx \frac{\partial M(\lambda, T)}{\partial T} \Delta T.$$

Then signal-to-noise relation $q_1 = \frac{\Delta U}{U_u}$ taking into account (2) will be of the form:

$$q_1(\lambda) = \frac{A_3 \cdot A_0 \cdot D_{\max}^* \cdot \tau_o}{\pi \cdot L^2 \cdot \sqrt{A_e \cdot \Delta f}} \Delta T \cdot \int_{\lambda_1}^{\lambda_2} \frac{\partial M(\lambda, T)}{\partial T} \cdot e^{-\alpha(\lambda)L} \cdot d\lambda. \quad (3)$$

The dependence of the attenuation natural indicator $\alpha(\lambda)$ on EMS length at the molecular or aerosol mechanisms of scattering and absorption is interpreted by G. Mie's known theory of radiation scattering in the turbid environment, which is based on the classical Maxwell's equations and is represented by rather complex mathematical expressions containing a number of special functions

[30]. In this form, non-numerical integration in (3) is impossible. In practice, a somewhat approximate semi-empirical formula is used [31-33]:

$$\alpha(\lambda) = A\lambda^{-\beta}, \tag{4}$$

where $A = \frac{3.91}{S_M} (0.555)^\beta$,

S_M – meteorological visibility range, km.

In the general case the value of indicator β and depends on the state of the atmosphere. Value $\beta=4$ corresponds to molecular (Rayleigh) scattering and in EMS IR-range is neglected small. Value $\beta<4$ corresponds to the attenuation of radiation due to absorption and scattering on aerosol particles of the atmosphere.

Value β can be roughly compared with meteorological visibility S_M according to the characteristics of the atmosphere in terms of the International Classification [34, 35]:

- the atmosphere is cloudless, very clear: $S_M > 20km$, $\beta \in (3.4)$;
- cloudless, clear: $10km \leq S_M \leq 20km$, $\beta \in (2.3)$;
- noticeable haze, strong haze: $2km < S_M \leq 6km$, $\beta \in (1.5)$;
- light fog: $0.5km < S_M < 1km$, $\beta = 1$;
- thick, continuous fog: $0.05km < S_M < 0.2km$, $\beta \approx 0$.

In many cases dependence $\beta = 0.585 \cdot S_M^{1/3}$ is used, and under the conditions of moderate haze for $\lambda \in (0.61 \div 11.48) \mu m$ indicator $\beta \in 0.7$ [36, 37]. At operation sections $\lambda \in [8 \div 14] \mu m$, where most TID function, dependence of β on λ is weak, therefore, without a great error, value $\alpha(\lambda)$ can be characterized by average value $\bar{\alpha}$ at interval $\Delta\lambda = \lambda_2 - \lambda_1$, taking into account (4) (Figure 1):

$$\bar{\alpha}(\lambda_1, \Delta\lambda) = \frac{1}{\lambda_2 - \lambda_1} \int_{\lambda_1}^{\lambda_2} \alpha(\lambda) d\lambda = \frac{A}{(1-\beta) \cdot \Delta\lambda} \cdot [(\lambda_1 + \Delta\lambda)^{1-\beta} - \lambda_1^{1-\beta}], \beta \neq 1. \tag{5}$$

Then expression (3) will be of the form:

$$q_1(\lambda_1) = C_0 \cdot e^{-\bar{\alpha}(\lambda_1)L} \cdot \frac{\Delta T}{L^2} \cdot \int_{\lambda_1}^{\lambda_2} \frac{\partial M(\lambda, T)}{\partial T} d\lambda, \tag{6}$$

where $C_0 = \frac{A_3 \cdot A_0 \cdot \bar{M}_{max}^* \cdot \tau_0}{\pi \cdot \sqrt{A_e \cdot \Delta f}}$.

In the range of temperatures (250÷350)°K and wave lengths (1÷15) μm $\exp\left(\frac{C_2}{\lambda T}\right)$ takes the value within limits (15÷10²⁵). At lower temperatures, the exponent grows even more significantly. That is, in the range of functional lengths of EMS of thermal imagers of different generations, the spectral energy luminosity of the object and the background can be considered under the condition $\exp\left(\frac{C_2}{\lambda T}\right) \gg 1$,

which approximates Planck's formula by Wine's law and derivative in (6) $\frac{\partial M(\lambda, T)}{\partial T} \cong \frac{C_1 C_2}{T^2 \lambda^6} \cdot \exp\left(-\frac{C_2}{\lambda T}\right)$ (Figure 2).

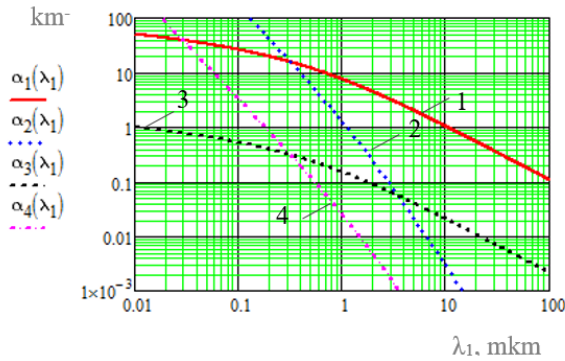


Figure 1. Dependence of the average natural index of atmospheric attenuation on fixed beginning λ_1 of the section of TID thermal sensitivity (curve 1 – SM=0.2 km, $\beta=1$; curve 2 – SM=0.2 km, $\beta=3$; curve 3 – SM=10 km, $\beta=1$; curve 4 – SM=10 km, $\beta=3$).



Figure 2. Spectral density of energy luminosity according to Planck's law (curve 1, 3 – solid) according to Wine's law (curves 2, 4 – dotted) at $T=350^\circ\text{K}$ (curves 1, 2) and $T=273^\circ\text{K}$ (curves 3, 4).

Taking into account the above said, relation (6) is of the form:

$$q_1(\lambda_1, T, \Delta T, \Delta \lambda) = \frac{C_0 \cdot C_1 \cdot T^3 \cdot \Delta T}{C_2^4 \cdot L^2} \cdot e^{-\bar{\alpha}(\lambda_1)L} \cdot \sum_{n=1}^2 (-1)^n \cdot e^{-x_n} \cdot (x_n^4 + 4x_n^3 + 12x_n^2 + 24x_n + 24), \quad (7)$$

where $x_n = \frac{C_2}{\lambda_n T}$, $\lambda_2 = \lambda_1 + \Delta \lambda$.

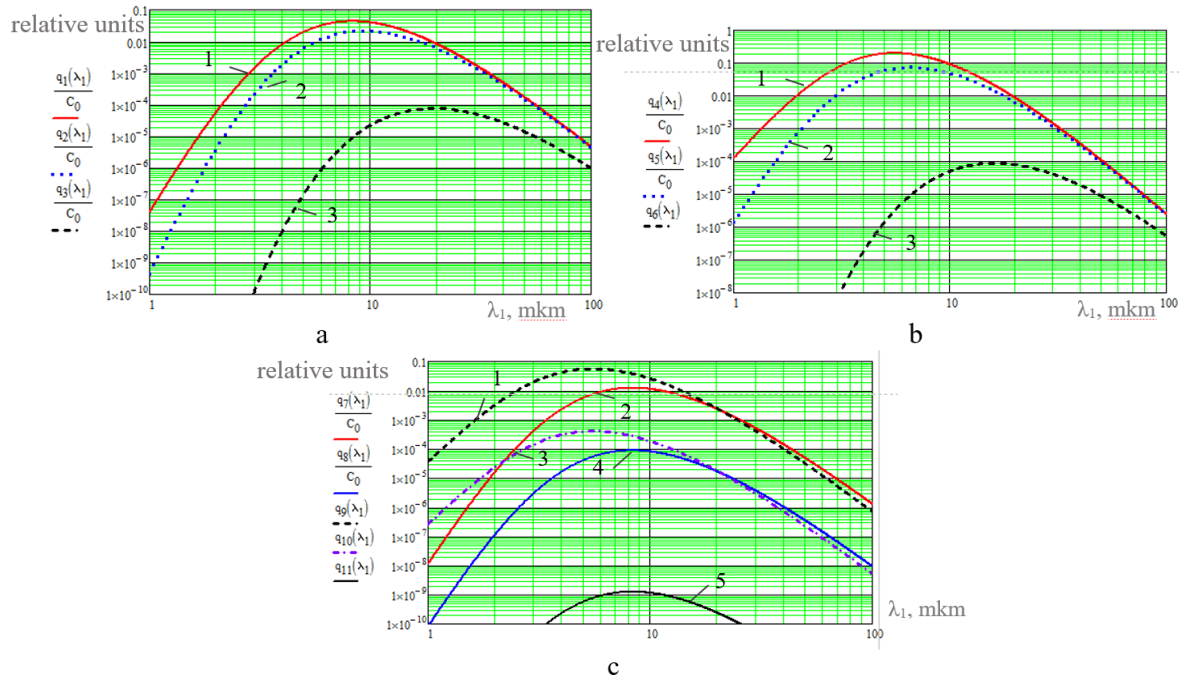


Figure 3. relation signal/noise at the output of TID receiver:

- a) $T=273^\circ\text{K}$; $\Delta T=1^\circ\text{K}$; $L=3$ km
(curve 1 – SM=30 km, $\beta=3.5$; curve 2 – SM=1 km, $\beta=1$; curve 3 – SM=0.2 km, $\beta=0.7$)
- b) curves 1, 2, 3 at $T=400^\circ\text{K}$
- c) $\beta=0$; $\Delta T=1^\circ\text{K}$; SM=0.2 km
($T=273^\circ\text{K}$: curve 1 – $L=0.3$ km; curve 3 – $L=0.5$ km; curve 5 – $L=1$ km
 $T=400^\circ\text{K}$: curve 2 – $L=0.3$ km; curve 4 – $L=0.5$ km).

As can be seen from Figure 3, the maximum signal-to-noise ratio at the output of the receiver is shifted to the long-wavelength section of the IR range with decreasing β , that is, with impaired visibility. At $\beta=0$ relation q/C_0 does not depend on λ_1 , but its value at a distance of $L=3$ km is very small and it becomes significant only at distances $L \leq 0.2$ km. The higher the temperature of the object and the background is the more $\max q(\lambda_1)$ shifts into the short wavelength range. When temperature T changes within the limits of $273^\circ\text{K} \div 400^\circ\text{K}$, and S_M from 0.2 km to 30 km, $\max q(\lambda_1)$ is within the limits $\sim (5 \div 12) \mu\text{m}$. That is, at high T (and available ΔT) objects can be detected by TID with receiver sensitivity in the range of $\lambda_1 \sim 5 \mu\text{m}$. At low T greater detection efficiency will be observed at longer operating waves. Fig. 3 illustrates the fact that with deterioration of visibility from $S_M \geq 20$ km to $S_M \leq 0.2$ km the probability of detecting objects for devices with short-wave sensitivity decreases and detection may not be possible at all, while for devices with long-wave sensitivity it may be most effective.

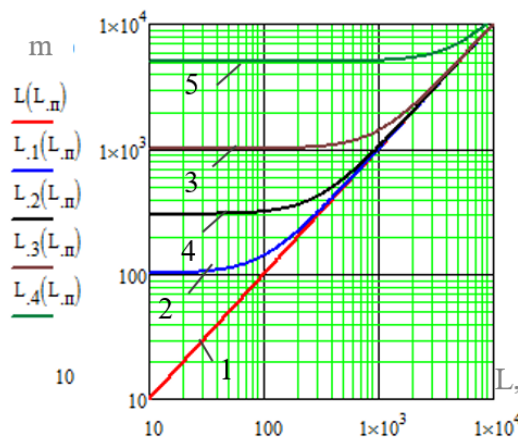


Figure 4. Dependence of the detection range of the object by the thermal imager on the distance caused by the illumination curve 1 – $L_T=0$; curve 2 – $L_T=0.1$ km; curve 3 – $L_T=0.3$ km; curve 4 – $L_T=1$ km; curve 5 – $L_T=5$ km).

3.2. Optimization via the choice of the section of the atmosphere transmittance spectrum.

When the TID operates with the sensitivity of the receivers, parts of the spectrum of which are combined with the "windows" of the transparency of the atmosphere, indicator $\alpha(\lambda)$ is small and can be neglected [17, 18]. In the case inequality $\bar{\alpha}(\lambda_1) \ll L^{-1}$ is true and $\exp(-\bar{\alpha}(\lambda_1) \cdot L) \cong 1$, signal-to-noise relation q_2 at the output of the receiver increases by $\exp(\bar{\alpha}(\lambda_1) \cdot L)$ times.

3.3. "Illumination" of the observation zone by artificial sources of IR radiation.

Assume there are N IR ray diodes, whose operating wave lengths λ_i are on the section of TID thermal sensitivity. Then signal-to-noise relation at the receiver output will increase by value of $q_{1\text{mi}0}(r_i, \theta_i)$:

$$q_{1\text{mi}0}(r_i, \theta_i) = C_0 \cdot \sum_{i=1}^N \int_{\lambda_1}^{\lambda_2} \frac{I_i(\lambda, \theta_i) \cdot \cos \theta_i \cdot \rho_i(\theta_i)}{L^2 r_i^2} d\lambda \cdot e^{-\alpha(\lambda_i)(L+r_i)}, \tag{8}$$

where $I_i(\lambda, \theta_i)$ – the spectral density of the radiant intensity of the i -th source;

$\rho_i(\theta_i)$ – the coefficient of infrared rays reflection from the object;

θ_i – the polar distance of the beam direction from the i -th source;

r_i – the distance between the object of observation and the i -th radiation source.

In the general case, taking into account the "illumination", relation q_1^* signal-to-noise is:

$$q_1^*(\lambda_1, T, \Delta T, \Delta \lambda, r_i, \theta_i) = q_1(\lambda_1, T, \Delta T, \Delta \lambda) + q_{1\text{mi}0}(r_i, \theta_i). \tag{9}$$

When combining the spectral sensitivity of the receiver, the "transparency windows" of the atmosphere and the emission spectra of the ray diodes ($\bar{\alpha}(\lambda_1) \ll L^{-1}, r_i^{-1}$) signal-to-noise relation q_2^* is:

$$q_2^*(\lambda_1, T, \Delta T, \Delta \lambda, r_i, \theta_i) = q_2(\lambda_1, T, \Delta T, \Delta \lambda) + q_{2n\bar{i}o}(r_i, \theta_i), \tag{10}$$

where $q_{2n\bar{i}o}(r_i, \theta_i) = C_0 \cdot \sum_{i=1}^N \cdot \int_{\lambda_1}^{\lambda_2} \frac{I_{oi}(\lambda) f_i(\theta_i) \cdot \cos \theta_i \cdot \rho_i(\theta_i)}{L^2 r_i^2} d\lambda$

Without detailed calculation of $q_{1n\bar{i}o}$ and $q_{2n\bar{i}o}$, which is a separate problem, we can estimate the contribution of illumination to the detection range of an aircraft object. Solving equation (10) with respect to L at $q_2^* = 1$, we have:

$$L = \sqrt{L_T^2 + L_{n\bar{i}o}^2}, \tag{11}$$

where $L_T = \left[\frac{C_0 C_1 \cdot T^3 \cdot \Delta T}{C_2^4} \sum_{n=1}^2 (-1)^n \cdot e^{-x_n} (x_n^4 + 4x_n^3 + 12x_n^2 + 24x_n + 24) \right]^{1/2}$ – range of detection of TID

object due to its thermal radiation without "illumination";

$$L_{n\bar{i}o} = \left(C_0 \cdot \sum_{i=1}^N \cdot \int_{\lambda_1}^{\lambda_2} \frac{I_i(\lambda, \theta_i) \cdot \cos \theta_i \cdot \rho_i(\theta_i)}{r_i^2} d\lambda \right)^{1/2}$$
 – increase in the detection range of the TID object

due to additional "illumination" of the object (Figure 4).

It is easily seen that $L_{n\bar{i}o}$ can vary widely, reaching a value predominant over L_T and can be the only factor in the detection of UAVs with low intrinsic thermal radiation. The detection range of the object can be increased by adjusting intensity $I_i(\lambda)$. For the continuity of the detection zone, the searchlights are selected to the required power and pattern. Distance d between them is calculated based on the specified minimum height of the field overlap h_{min} :

$$d = 2h_{min} \cdot tg \gamma; \tag{12}$$

where γ – the aperture angle of searchlight emission.

The active work of EMS sources is a factor in unmasking their positions, however, the placement of a significant number of infrared searchlights in a large area is at the same time a disorientation for enemy air reconnaissance.

The use of a large number of IR searchlights to illuminate UAVs operating in areas of the thermal sensitivity spectrum of TID and located over a large area is nothing more than an analogue of multi-position multistatic radar [36-44].

4. Conclusions.

1. With decreasing meteorological visibility S_M the maximum signal from the TID receiver is shifted to the long-wavelength part of the IR spectrum.

2. At low visibility ($S_M \leq 0.2km$) TIDs with long-wavelength sensitivity in the IR range have advantages in object detection at long distances.

Surveillance devices with short-wave sensitivity in the IR range can be effective at short distances.

3. The use of infrared searchlights to illuminate the air surveillance zone, the combination of searchlight emission spectra, thermal sensitivity of TID and "windows of transparency" of the atmosphere can significantly increase the efficiency of UAV detection.

References

- [1] Surianinov M and Krutii Y 2018 To the solution of the problem of bending of a cylindrical shell by the boundary elements method *MATEC Web of Conferences* **230** 02032 doi:10.1051/mateconf/201823002032
- [2] Krutii Y, Suriyaninov M and Vandynskiy V 2018 Analytic formulas for the natural frequencies of hinged structures with taking into account the dead weight *MATEC Web of Conferences* **230** doi:10.1051/mateconf/201823002016
- [3] Bast J, Gorbatyuk S M and Kryukov I Yu 2011 Horizontal hcc-12000 unit for the continuous casting of semifinished products *Metallurgist* **55 (1-2)** pp 116–118 doi:10.1007/s11015-011-9399-1
- [4] Romanchenko I S, Zahorka O M, Butenko O V and Deineha O V 2011 Theory and practice of combating small low-flying objects *Assessment of capabilities, trends in the development of air defense monograph* (Zhytomyr: Polissia) 344
- [5] Shapoval A, Savchenko I and Markov O 2021 Determination coefficient of stress concentration using a conformed display on a circle of a single radius *Solid State Phenomena* **316** pp 928–935
- [6] Vladov S, Shmelov Y and Shmelova T 2020 Modeling of the TV3-117 aircraft engine technical state as part of the helicopter power plant in the form of the markov process of death and reproduction *CEUR Workshop Proceedings* **2740** pp 400–407
- [7] Danyk Yu H and Buhaiov M V 2015 Analysis of the effectiveness of detecting tactical unmanned aerial vehicles by passive and active means of surveillance *Collection of papers of ZhVI DUT* **10** pp 5–20
- [8] Markov O E, Gerasimenko O V, Shapoval A A, Abdulov O R and Zhytnikov R U 2019 Computerized simulation of shortened ingots with a controlled crystallization for manufacturing of high-quality forgings *International Journal of Advanced Manufacturing Technology* **103(5-8)** pp 3057–3065
- [9] Osadchiy V A, Albul S V, Kuprienko N S and Kirillova N L 2020 Future developments of a roll forming mill design algorithm *IOP Conference Series: Materials Science and Engineering* **709 (4)** 044079 doi:10.1088/1757-899X/709/4/044079
- [10] Kukhar V V, Grushko A V and Vishtak I V 2018 Shape indexes for dieless forming of the elongated forgings with sharpened end by tensile drawing with rupture *Solid State Phenomena* **284** pp 408–415 doi:10.4028/www.scientific.net/SSP.284.408
- [11] Khudov H V, Misiuk H V, Oleksenko O O, Raikov R Yu, Bezklubenko O O and Dobrev V Yu 2018 Analysis of existing ways to increase the efficiency of detection of small air objects by radar means of airspace control *Control, navigation and communication systems* **6(52)** pp 38–42
- [12] Naumova M G, Morozova I G and Borisov P V 2020 Study of metal surface with color image obtained with laser marking *Solid State Phenomena* **299** pp 943–948 doi:10.4028/www.scientific.net/SSP.299.943
- [13] Grushko A V, Kukhar V V and Slobodyanyuk Y O 2017 Phenomenological model of low-carbon steels hardening during multistage drawing *Solid State Phenomena* **265** pp 114–123 doi:10.4028/www.scientific.net/SSP.265.114
- [14] Shapoval A, Drahobetskyi V, Savchenko I, Gurenko A and Markov O 2020 Profitability of production of stainless steel + zirconium metals combination adapters *Key Engineering Materials* **864** pp 285–291
- [15] Shmelova T, Shmelov Y and Vladov S 2020 Concept of Building Intelligent Control Systems for Aircraft, Unmanned Aerial Vehicles and Aircraft Engines *IEEE 6th International Conference on Methods and Systems of Navigation and Motion Control, MSNMC 2020 – Proceedings* pp 14–19

- [16] Kovalevskiy S M, Tiutiunnik V O and Khudov H V 2015 Method for calculating the scattering surface efficiency of small air objects with single-position and spaced signal reception in survey radar stations *Collection of papers of Kharkiv University of Aviation* **2(43)** pp 28–31
- [17] Lukianova T, Donenko V and Klein R 2020 Implementing Building Information Modelling for the Reconstruction Process of Unfinished Building Projects *IEEE European Technology and Engineering Management Summit, E-TEMS 2020* 9111794
- [18] Kobelev O A, Albul S V and Kirillova N L 2020 Research and development of broaching methods on mandrel of large-sized pipe forgings *IOP Conference Series: Materials Science and Engineering* **709** (4) 044104 doi:10.1088/1757-899X/709/4/044104
- [19] Zarapin A Yu, Shur A I and Chichenev N A 1999 Improvement of the unit for rolling aluminum strip clad with corrosion-resistant steel *Steel in Translation* **29** (10) pp 69–71
- [20] Savchenko I, Shapoval A and Gurenko A 2020 Modeling dynamic parameters of hard alloys during shock wave regeneration *IOP Conference Series: Materials Science and Engineering* **969(1)** 012079
- [21] Artiukh V, Mazur V and Adamtsevich A 2017 Priority influence of horizontal forces at rolling on operation of main sheet rolling equipment *MATEC Web of Conferences* **106** 04001 doi:10.1051/mateconf/201710604001
- [22] Volkov VH 2006 Aviation night vision devices *Special equipment* **4** pp 2–12
- [23] Starodubov A V, Serdobintsev A A, Kozhevnikov I O, Pavlov A M, Galushka V V, Torgashov R A, Bessonov D A, Galkin A, Ryskin N M and Sakharov V K 2020 Comparison of nanoseconds and picoseconds laser ablation for microfabrication of planar slow-wave structures for D-band vacuum electronic devices with sheet electron beam *Progress in Biomedical Optics and Imaging - Proceedings of SPIE* **11458** 1145803 doi:10.1117/12.2564423
- [24] Shmelov Y, Vladov S, Klimova Y and Kirukhina M 2018 Expert system for identification of the technical state of the aircraft engine TV3-117 in flight modes *IEEE 1st International Conference on System Analysis and Intelligent Computing, SAIC 2018 – Proceedings* **8516864**
- [25] Volkov V H 2006 Ship night vision devices *Special equipment* **1** pp 2–8
- [26] Sereda B, Sheyko S, Belokon Y and Sereda D 2011 The influence of modification on structure and properties of rapid steel *Paper presented at the AIST Steel Properties and Applications Conference Proceedings – Combined with MS and T'11 (Mater. Sci. and Tech. 2011)* pp 457–460
- [27] Hrudkina N, Aliieva L, Markov O, Marchenko I, Shapoval A, Abhari P and Kordenko M 2020 Predicting the shape formation of hollow parts with a flange in the process of combined radial-reverse extrusion *Eastern-European Journal of Enterprise Technologies* **4/1** (106) pp 55–62
- [28] Shvab'yuk V I, Krutii Y S and Sur'yaninov M G 2016 Investigation of the Free Vibrations of Bar Elements with Variable Parameters Using the Direct Integration Method *Strength of Materials* **48** (3) pp 384–393 doi:10.1007/s11223-016-9776-x
- [29] Volkov VH 2001 New generation ship night vision devices *Special equipment* **5** pp 2–8
- [30] Dragobetskii V V, Shapoval A A, Mospan D V, Trotsko O V and Lotus V V 2015 Excavator bucket teeth strengthening using a plastic explosive deformation *Metallurgical and Mining Industry* **7** (4) pp 363–368
- [31] Markov O, Gerasimenko O, Aliieva L and Shapoval A 2019 Development of the metal rheology model of high-temperature deformation for modeling by finite element method *EUREKA, Physics and Engineering* **2** pp 52–60
- [32] Petrunenko I V, Belei S I, Petchenko M V, Bodnar O A and Maslak N G 2020 Organizational and financial principles for the development of euroregions *International Journal of Economics and Business Administration* **8(3)** pp 150–160

- [33] Norton Y, Cambell S Horn D end Reago P 2000 Third generation imaging *Proc. SPJE* **4130** pp 226–235
- [34] Keropyan A M 2016 Features of interaction of traction wheels of an electric locomotive and a diesel locomotive with rails in the conditions of open mountain works *Journal of Friction and Wear* **37** (1) pp 78–82 doi:10.3103/S1068366616010074
- [35] Kondratenko V V, Sedykh L V, Mirzakarimov A and Aleksakhin A 2020 Static analysis and strength calculation of drive shaft of large-scale cone crusher *E3S Web of Conferences* **193** 01038 doi:10.1051/e3sconf/202019301038
- [36] Malinov L S, Malysheva I E, Klimov E S, Kukhar V V and Balalayeva E Yu 2019 Effect of Particular Combinations of Quenching, Tempering and Carburization on Abrasive Wear of Low-Carbon Manganese Steels with Metastable Austenite *Materials Science Forum* **945** pp 574–578 doi.org/10.4028/www.scientific.net/MSF.945.574
- [37] Shapoval A, Kantemyrova R, Markov O, Chernysh A, Vakulenko R and Savchenko I 2020 Technology of production of refractory composites for plasma technologies *Proceedings of the 25th IEEE Int. Conf. on Problems of Automated Electric Drive Theory and Practice* **9240830** 2020 doi:10.1109/PAEP49887.2020.9240830.
- [38] Mykytenko V I and Kotovskyi V I 2008 Remote observations in the fog using passive two-channel iconic optoelectronic systems Methods and systems of optoelectronic and digital signal processing **35** pp 29–37
- [39] Zagirnyak M, Zagirnyak V, Moloshtan D, Drahobetskyi V and Shapoval A 2019 A search for technologies implementing a high fighting efficiency of the multilayered elements of military equipment *Eastern-European Journal of Enterprise Technologies* **6** (1-102) pp 33–40 doi:10.15587/1729-4061.2019.183269
- [40] Larin S N, Platonov V I and Solomonov K N 2017 Approach to assessment of microdamages accumulated during the constrained molding of shells made of the material subject to energy theory of creep and damage *Journal of Chemical Technology and Metallurgy* **52** (4) pp 679–684
- [41] Oliinyk A, Fedorchenko I, Donenko V, Korniienko S and Kharchenko A 2020 Development of an Evolutionary Optimization Method for Financial Indicators of Pharmacies *International Journal of Computing* **19(3)** pp 449–463
- [42] Khrebtova O A, Shapoval A A, Mos'pan D V, Dragobetsky V V, Gorbatyuk S M and Markov O E 2021 Automatic temperature control system for electrocontact annealing of steel welding wire *Metallurgist* **65** (3–4)
- [43] Markov O E, Kukhar V V, Zlygoriev V N, Shapoval A A, Khvashchynskyi A S and Zhytnikov R U 2020 Improvement of Upsetting Process of Four-Beam Workpieces Based on Computerized and Physical Modeling *FME Transactions* **48** (4) pp 946–953 doi:10.5937/fme2004946M
- [44] Kolobrodov V H and Lykholit M I 2007 Design of thermal imaging and television surveillance systems *Textbook* 364